Luminescent Water Dispersible Microporous Polymeric Nanospheres

Alex M. James [a], Matthew J. Derry [a], Jennifer S. Train [a] and Robert Dawson*[a]
Department of Chemistry, University of Sheffield, Brook Hill, Sheffield S3 7HF

ABSTRACT: Water-dispersible porous polymeric dispersions (PPDs) have been synthesised by reversible addition-fragmentation chain transfer mediated polymerisation-induced self-assembly (RAFT-mediated PISA). The core-shell particles posses a microporous core formed from divinylbenzene and fumaronitrile while the outer polyethylene glycol shell enables the particles to be dispersible in a wide range of solvents. The PPD was shown to have a heirarchical structure of small primary nanoparticles within larger, well-defined aggregates of 220 nm as measured by electron microscopy and small angle x-ray scattering (SAXS) and exhibited a surface area of 274 m^2/g. Furthermore these samples were found to be fluoresent and demonstrate selective detection of harmful nitroaramatics in solution with extremly low limits of detection, 169 ppb for picric acid, as well as possessing a CO_2 uptake of 1.1 mmol/g at 273 K.

Introduction

The design and synthesis of microporous organic polymers (MOPs) is a growing area of research due to a combination of properties which include high surface area, chemical and thermal stability, low skeletal density and relative ease with which they can be functionalised, either by the judicious use of pre-functionalised monomers or via post-synthetic modification towards more complex functionalities.[1] The combination of these properties has attracted considerable interest not only in fundamental research but also into the practical application of these materials in fields such as gas separation[2–7], chemosensing[8–11], waste-water treatment[12,13] and catalysis.[14,15] Amongst MOPs many subclasses exist including polymers of intrinsic microporosity (PIMs)[16–21], conjugated microporous polymers (CMPs)[22–26], covalent organic frameworks (COFs)[27–30] and covalent triazine-based frameworks (CTFs)[31,32] to name but a few. However, there are a number of disadvantages to some of these material sub-classes, such as the need for expensive monomers, metal catalysts and lengthy polymerisation times which limits their use in many practical applications.

Hypercrosslinked polymers (HCPs)[32–37] represent a subclass of MOPs which don't suffer from the aforementioned issues described above. HCP synthesis is facile, quick and utilises cheap starting materials which ensures ease of scalability. One common way of synthesising HCPs from aromatic building is through the exploitation of external crosslinkers such as formaldehyde dimethyl acetal (FDA).[38] This method exploits Friedel-Crafts alkylation chemistry using iron(III) chloride as the catalyst thus ensuring permanent porosity and achieving high surface areas in the final products. These materials are however not without their drawbacks, which include the use of 1,2-dichloroethane as the solvent and residual iron contaminants which can be difficult to fully remove from the pores of the sample.

One key disadvantage to most MOPs (with the exception of some PIMs) is their complete insolubility in all solvents. This is due to their highly crosslinked structure which is necessary to induce porosity in these materials. PIMs avoid this problem by using a rigid and contorted monomer which allows soluble microporous polymers to be produced and cast into free standing films. This does however have its own disadvantage in the fact that there are only a few of these rigid contorted monomers available commercially. A number of other attempts have led to the fabrication of solution-processable microporous polymers including; the addition of solubilising side chains to monomers such as tetraphenyl5,5-dioctylcyclopentadiene.[39] However, the long flexible chains that provide the solubility also fill the pores of the material resulting in a very low surface area. Cheng *et al*. used pyrene based monomers with solubilising t-butyl groups to produce a soluble CMP network using Suzuki coupling, however this route requires the use of expensive Pd catalysts and has a limited range of t-butyl monomers which can be used.[40] By using high dilution Yang *et al.* were able to hypercrosslink individual poly(styrene) chains which were found to be soluble in a range of solvents with surface areas up to around 700 m^2/g.[41] Though these porous polymers were found to lose their porosity over time. Mai *et al*. were able to synthesise microporous particles using a divergent 3-step procedure by firstly making vinylbenzyl chloride particles using emulsion polymerisation followed by hypercrosslinking with $FeCl_3$ in 1,2,dichloroethane.[42] Using the unreacted end groups it was possible to grow solubilising polymer chains *via* ATRP chemistry resulting in a core-shell structure with a surface area of 562 m^2/g. While this route demonstrated the concept of core-shell microporous particle dispersions, the use of the multi-step approach, harmful solvents and stoichiometric amounts of $FeCl_3$ is not ideal and due to the acidic conditions limits the possibility of functionalisation. The synthesis of soluble or dispersible microporous polymers is however, clearly still of great importance. Equally

important is the need to develop a more generic method of synthesising MOPs which alleviates these issues and delivers a material which is able to be processed and applied in the solution form from simple building blocks in a one pot synthesis.

Recently, the group of Li and co-workers reported the synthesis of a series of microporous polymers from the widely available vinyl precursors divinylbenzene and fumaronitrile *via* conventional radical polymerisation thus avoiding some of the issues attributed to conventional HCP synthesis.[43] These polymers boast large surface areas as well as being cheap to synthesise. Furthermore, no by-products are formed from the reaction and there is no need for metal-catalysts or harmful solvents to be used in order to induce porosity. Yet, like most porous materials, they are completely insoluble in common organic solvents, hence limiting their potential applications.

We believe that the strategy of using block copolymers to provide a porous core and an outer shell block to disperse the particles has significant scope for variation to produce a wide variety of dispersible microporous particles. Here, we report, for the first time, the synthesis of porous polymeric dispersions (PPDs) synthesised *via* a radical addition fragmentation transfer-mediated polymerisation induced self-assembly (RAFT-mediated PISA) approach using a water soluble macro-chain transfer agent (CTA).

Experimental

Materials

Poly(ethylene glycol) methyl ether (PEG, Mn 5000, PDI 1.09), anhydrous trimethylamine (TEA), 2-bromoisobutyryl bromide, dodecane thiol, potassium phosphate tribasic (K_3PO_4), Fumaronitrile (FN, 98 %) and potassium persulfate were all purchased from Sigma-Aldrich and used as received. Dry toluene was obtained in a method analogous to the one outlined by Grubbs.[44] Magnesium sulfate and carbon disulphide were purchased from Fischer and used as received. Divinylbenzene (DVB, technical grade 80 %) was passed through an alumina column in order to remove the inhibitor before use. Fumaronitrile (FN, 98 %) and 2,2′-Azobis(2-methylpropionitrile) (AIBN, 98 %) were purchased from Sigma-Aldrich and used without further purification. All other chemicals were purchased from Sigma-Aldrich and used without any further purification.

Synthesis of PEG113-Br

PEG_{113}-Br was prepared in a method similar to that reported by M. Liu and co-workers.45 PEG_{113} (8 g, 1.6 mmol, 1 eq.) was dissolved in anhydrous toluene (100 mL) in a two-neck flask. TEA (0.32 mL, 2.3 mmol, 1.4 eq.) was added and the solution was cooled to 0 °C. 2-bromoisobutyryl bromide (0.26 mL, 2.1 mmol, 1.3 eq.) was added dropwise over the course of 1 h before being left to stir overnight at room temperature. The solvent was reduced before being precipitated into an excess of cold diethyl ether (200 mL). The crude product was dried under vacuum, dissolved in water before being extracted with DCM. The organic layers were collected, combined and dried over $MgSO_4$ and placed the fridge overnight to obtain the PEG_{113}-Br product.

Synthesis of PEG-based macro-chain transfer agent (CTA)

The PEG-based macro-CTA was synthesised using a method adapted from a paper published by O'Reilly and co-workers.[46] Dodecane thiol (0.60 mL, 2.5 mmol, 1 eq.) was added to a stirred suspension of K_3PO_4 (0.53 g, 2.5 mmol, 1 eq.) in acetone (50 mL) and stirred for 10 minutes. Carbon disulphide (0.36 mL, 6 mmol, 2.5 eq.) was added to the suspension and left to stir for a further 10 minutes. PEG_{113}-Br (10 g, 2 mmol, 0.8 eq.) in acetone (30 mL) was added to the suspension which was left to stir overnight at room temperature. The solvent was removed by rotary evaporation precipitated into an excess of n-hexane twice and once into diethyl ether to ensure purity. The sample was dried in the vacuum oven overnight at 40 °C to afford the RAFT macro-CTA.

Synthesis of FN/DVB insoluble analogue

The insoluble porous polymer of FN/DVB was synthesised in an identical method to that reported by Li and co-workers.[43] DVB (0.26 g, 2 mmol, 1 eq.), FN (0.117 g, 1.5 mmol, 0.75 eq.) and toluene (10 mL) were all added to a 2-neck round bottom flask under nitrogen. The flask was heated to 80 °C and polymerisation was initiated through the addition of AIBN (3.8 mg, 0.023 mmol, 0.01 eq.). After 24 h the polymerisation was quenched and the solution poured into methanol to precipitate the polymer. The solid was washed with methanol and tetrahydrofuran (THF) and extracted from THF in Soxhlet apparatus for 16 h. The final product was collected and dried under vacuum at 60 °C.

Synthesis of PEG-b-PDVB-co-PFN via RAFT mediated polymerisation

A RAFT-mediated polymerisation route was employed utilising the PEG-based macro. The PEG-based macro CTA (0.13 g, 0.2 mmol, 1 eq.) and FN (0.35 g, 4.5 mmol, 18 eq.) were added to a 2-necked round bottom flask. The flask was evacuated and back-filled with nitrogen 3 times. Toluene (30 mL) and DVB (0.85 mL, 6 mmol, 24 eq.) were added to the flask to create a 5 % wt. solution. The solution was bubbled through with nitrogen gas to ensure the system was devoid of air before heating to 70 °C. Polymerisation was initiated through the addition of AIBN (4 mg, 0.25 mmol, 0.1 eq) and held at 70 °C for 24 h. The solid was washed with methanol and tetrahydrofuran (THF) and extracted from THF in Soxhlet apparatus for 16 h. The final product was collected and dried under vacuum at 60 °C.

Synthesis of PEG-b-PDVB-co-PFN Porous Dispersions

A RAFT-mediated PISA approach was applied in order to synthesise a series of porous nanoassemblies through varying the solvent ratio of water:ethanol. The PEG-based macro CTA (0.13 g, 0.2 mmol, 1 eq.) and FN (0.35 g, 4.5 mmol, 18 eq.) were added to a 2-necked round bottom flask. The flask was evacuated and back-filled with nitrogen 3 times. Water and ethanol of varying ratios along with DVB (0.85 ml, 6 mmol, 24 eq.) were added to the flask to

create a 1 % wt. solution. The solution was bubbled through with nitrogen gas to ensure the system was devoid of air before heating to 70 °C. Polymerisation was initiated through the addition of potassium persulfate (KPS, 4 mg, 0.025 mmol, 0.1 eq.) and held at 70 °C for 24 h. The product was isolated as a white solid through reprecipitation into diethyl ether before drying in vacuo at 40 °C for 16 h. The obtained polymers were labelled as PPD-x. A table showing the preparation of each PPD is listed in table S1.

Preparation of PPDs solutions for use in fluorescence studies

A 100 cm^3 stock solution containing 1 mg of the PPD in methanol was prepared. This optical density of this sample at 275 nm was found to be 0.2. 2.5 cm^3 of this sample was added to a glass cuvette which was used for the fluorescence studies. A separate 1 mM stock solution containing the quencher along with the PPD was also made up. This solution was added sequentially to the cuvette and the fluorescent quenching was observed.

Characterisation

Fourier transform infrared (FTIR) spectroscopy was performed using a Perkin-Elmer Spectrum 100 fitted with an attenuated total reflectance tip (ATR). ^{1}H- and ^{13}C- NMR spectra were recorded on a 400 MHz Bruker Avance-400 spectrometer. Molecular weights (Mn) and polydispersity indices (PDI) were measured by gel permeation chromatography (GPC). THF was used as the eluent with a flow rate of 1 mL min^{-1} at 25 °C using polystyrene as the calibration standard. Universal calibration was applied employing Erma ERC-7512 refractive index detectors using Cirrus GPC-online software for analysis. Dynamic light scattering (DLS) of the PPDs were carried out using a Malvern Zetasizer nanoZS instrument *via* the Stokes-Einstein equation which assumes perfectly monodisperse, non-interacting spheres.

Solid-State NMR samples were packed into 4 mm zirconia rotors and transferred to a Bruker Avance III HD spectrometer. 1D ^{1}H-^{13}C cross-polarisation magic angle spinning (CP/MAS) NMR experiments were measured at 125.76 MHz (500.13 MHz ^{1}H) at a MAS rate of 10.0 kHz. The ^{1}H $\pi/2$ pulse was 3.4 µs, and two-pulse phase modulation (TPPM) decoupling was used during the acquisition. The Hartmann-Hahn condition was set using hexamethylbenzene. The spectra were measured using a contact time of 2.0 ms. The relaxation delay D_1 for each sample was individually determined from the proton T_1 measurement ($D_1 = 5 \times T_1$). Samples were collected until sufficient signal to noise was observed, typically greater than 256 scans. The values of the chemical shifts are referred to that of TMS.

Scanning electron microscopy (SEM) images were collected on a Fei Inspect F50 Field Emission Gun SEM, run in secondary electron mode. Specimens were prepared by mounting onto carbon tape, supported on aluminium stubs. Transmission electron microscopy (TEM) studies were conducted using a Philips CM 100 instrument operating at 100 kV and equipped with a Gatan 1 k CCD camera. A diluted PPD solution (0.10% w/w) was placed on carbon-coated copper grids, allowed to dry and then exposed to ruthenium(VIII) oxide vapor for 7 min at 20 °C prior to analysis. The ruthenium(VIII) oxide was prepared as follows: Ruthenium(IV) oxide (0.30 g) was added to water (50 g) to form a black slurry; addition of sodium periodate (2.0 g) with stirring produced a yellow solution of ruthenium(VIII) oxide within 1 min.[47]

Small-angle X-ray scattering (SAXS). SAXS data were collected using a laboratory SAXS instrument (Xeuss 2.0, Xenocs, France) equipped with a liquid gallium MetalJet X-ray source (Excillum, Sweden, wavelength λ = 0.134 nm), two sets of motorized scatterless slits for beam collimation and a Dectris Pilatus 1M pixel detector (sample-to-detector distance 6.335 m). SAXS patterns were collected over a q range of 0.011 $nm^{-1} < q < 1.0$ nm^{-1}, where $q = (4\pi\sin\theta)/\lambda$ is the length of the scattering vector and θ is one-half of the scattering angle. Glass capillaries of 2 mm diameter were used as a sample holder and 6 data sets were collected over 10 min for each sample (empty capillary, methanol and 5% w/w PPD-5 in methanol). Data were reduced (normalization and integration) using the Foxtrot software package supplied with the instrument and further analysed (background subtraction and data modelling) using Irena SAS macros for Igor Pro.[48]

Gas sorption measurements were performed using a micromeritics ASAP 2020 plus analyser employing high purity gases. Samples were degassed at 120 °C for 16 h under vacuum immediately prior to analysis. UV-Vis absorption spectra were taken on a Cary 5000 spectrophotometer. All steady-state fluorescence spectra were recorded on a Horiba Jobin Yvon Fluoromax-4 spectrofluorometer. Time-resolved fluorescence spectroscopy of PPD samples dispersed in methanol was recorded on an Edinburgh instruments mini-tau compact fluorescence lifetime spectrometer containing a pulsed light source, sample chamber, integrated imaging components and a single photon detector. Data acquisition was carried out using T900 operating software. All samples were irradiated at 274.5 nm through an external LED pulsed light source, 75 ps.

Results and Discussion

To our knowledge, the synthesis of water-dispersible porous nanoassemblies has only been reported once before.[42] This method involved numerous synthetic steps, the use of multiple metal catalysts and environmentally harmful and carcinogenic solvents. In contrast to the particles synthesised by Mai *et al.*,[42] the use of a convergent RAFT-mediated PISA approach made possible the formation of a milky dispersion (scheme 1, PPD) from the copolymerisation of divinylbenzene and fumaronitrile in water/ethanol solvent mediated by a PEG macro-CTA. This method is versatile, metal-free, requires no harmful solvents and utilises cheap and readily available vinyl materials. Furthermore the synthesis is entirely one-pot, compatible with many different monomers and can be scaled-up with ease.

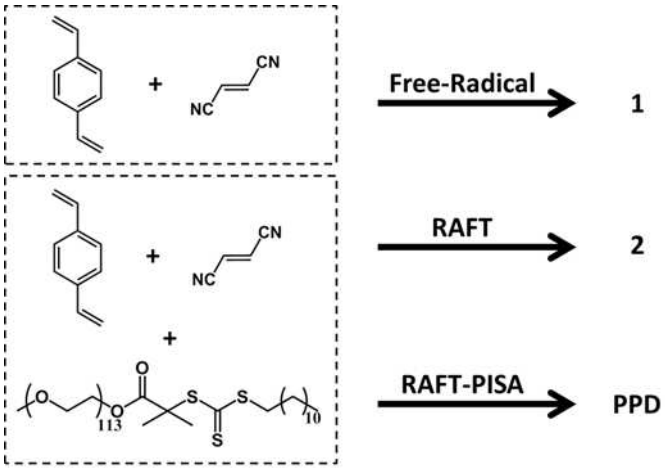

Scheme 1. Synthesis procedures used to fabricate microporous polymers via free radical polymerization (1), RAFT-mediated polymerization (2) and RAFT-medicated PISA (PPD).

In order to demonstrate the advantages of a RAFT-PISA synthesis route the PPD particles were compared the materials produced from the polymerisation of DVB/FN *via* two other routes. The first material involved the copolymerisation of FN/DVB *via* conventional free radical polymerisation (1) leading to a 3D porous network as demonstrated by Li and co-workers.[43] The second was a conventional RAFT-mediated approach in the presence of the PEG macro-CTA using toluene as the solvent media (2). Due to using toluene as the solvent no self-assembly was expected to occur as both the co-monomers and the PEG macro-CTA are soluble hence there is no driving force towards the self-assembly of particles of any morphology. Sample (1) was completely insoluble/dispersible and settled out of aqueous solution within 10 min. Sample 2 and the PPD were more dispersible as a result of the PEG chains. However, analysis of sample (2) by DLS was not possible demonstrating the lack of any regular particle sizes and after 16 hr this sample was shown to have settled out. The PPD sample in contrast remained dispersed in the solvent for many months without any noticeable sedimentation (Fig 1).

Precipitation of the PPD dispersion into diethyl ether allowed for the collection of a white solid which was found to be porous using the BET method. Redispersion of this material was possible using a wide range of common solvents (including water, alcohols, chloroalkanes, THF, acetonitrile and dioxane) after sonication.

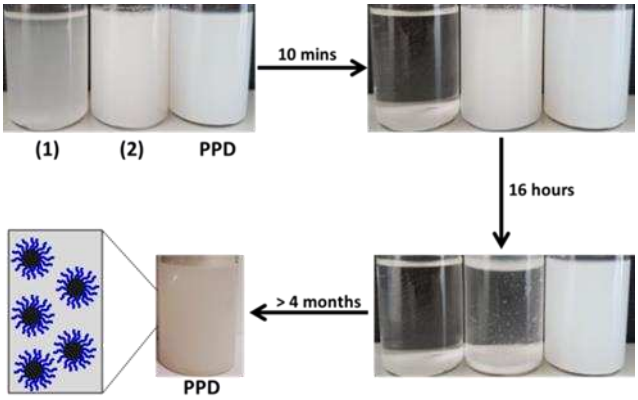

Figure 1. The dispersions of three polymer samples in water highlighting how the PPDs synthesised via the PISA approach remain in solution compared to those synthesised via conventional free radical polymerisation (1) and RAFT-mediated "linear" polymerisation (2)

In order to try and optimize the surface area and dispersibility 11 different samples were synthesised by varying the ratios of water to ethanol from 100:0 to 0:100 in increments of 10. All samples were found to be immediately dispersible though over time some samples did fall out of solution (Fig. S7). The optimum sample, which gave the largest surface area and was still dispersible, was found to be the sample synthesised in a 50:50 mix of water/ethanol. Hence all characterisation was carried out on this sample which is referred to as PPD-5.

PPD-5 was characterised in the solid state using the following techniques. FTIR (Fig. 2) analysis was carried out on the solid product and compared to those of the monomers. Comparison with the precursors showed clear signals from all three precursors at 2250, 1454 and 1125 cm^{-1}. These correspond to the C≡N of the fumaronitrile monomer, the C=C aromatic of divinylbenzene and the C-O vibrations from the PEG macro-CTA respectively.

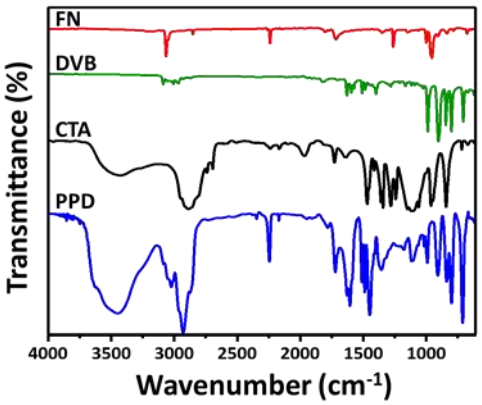

Figure 2. FTIR spectra of fumaronitrile (FN, red), divinylbenzene (DVB, green), PEG macro CTA (CTA, black) and PPD-5 (blue).

Elemental analysis of the samples (Table S2) after precipitation showed nitrogen contents between 5.73-9.44 %,

higher than the theoretical value (5.9 %) suggesting that the fumaronitrile has been incorporated into the product. Carbon and hydrogen values are also higher than expected, while the sulfur values are lower than expected. Together with the % yields, this leads to the assumption that not all of the macro-CTA has been incorporated into the final products.

Solution NMR (Fig. S6) of PPD-5 shows a single resonance in the 1H-NMR spectrum at 4.9 ppm which is attributed to the -CH_2- of the PEG chains. No other observable resonances were found, despite FTIR and elemental analysis indicating the successful polymerisation of fumaronitrile and divinylbenzene. Given that the aim of the polymerisation was to form a hypercrosslinked core, it is conceivable that it would be insoluble and hence undetectable via solution phase NMR. Solid state ^{13}C-CP/MAS NMR spectroscopy was therefore employed to further elucidate the structure of the PPD. A solid sample of the PPD was compared ¬with both the solution phase NMR spectrum and solid state insoluble FN/DVB analogue (1) and is presented in figure 3. The peaks at 143, 138, 129 and 117 ppm are attributed to the quaternary aromatic -C_{Ar}-, unreacted vinyl, aromatic -$C_{Ar\text{-}H}$ and the nitrile -C≡N groups. The peaks at 41 and 32 ppm are assigned to the -CH- and -CH_2- carbons of the polymer backbone respectively. Finally, the peak at 70 ppm, present only in the spectrum of the PPD sample, is ascribed to the carbon signals on the PEG chain similar to that observed in the solution phase spectrum.

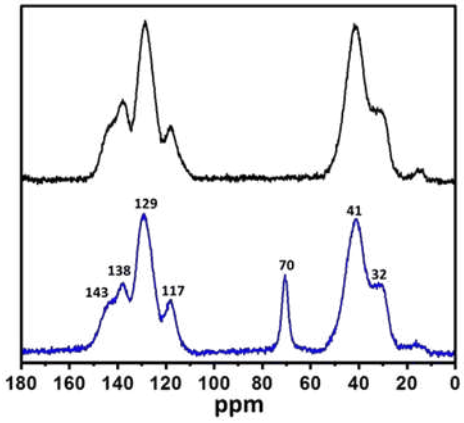

Figure 3. CP/MAS NMR spectra of (1) (black) and PPD (blue).

To investigate the size and morphology of the dispersions, DLS, TEM, SEM and SAXS were employed. The DLS measurements (Table S3, Fig. S8.) show that the sizes of the particles ranged from 300-500 nm for samples 1 to 8. Due to the crashing out of samples 9 to 11 it was not possible to obtain consistent measurements.

The range of particle sizes is independent of the solvent system though larger particles do seem to form when more ethanol is present. This apparent difference in diameter could be attributed to the miscibility of the monomers in the respective solvents. In water, DVB is completely immiscible hence an emulsion forms in which the DVB monomer forms emulsion droplets stabilised by the presence of the macro-CTA. However in ethanol, in which DVB is miscible, no such emulsion system forms. Hence, when polymerisation occurs, it could be assumed that the systems containing these emulsion droplets will yield a more monodisperse dispersion yet those in which emulsions do not preliminarily form will be more polydisperse. This could explain why larger particles are formed when ethanol dominates the solvent mixture.

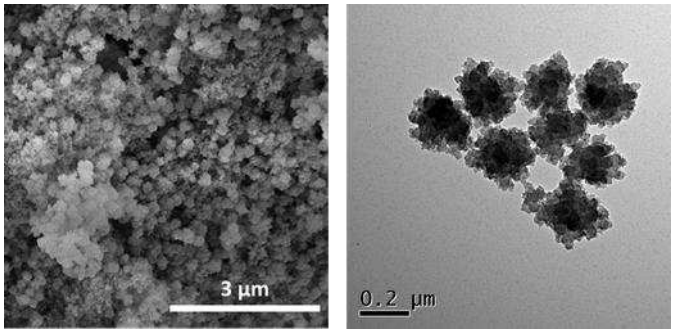

Figure 4. Electron microscopy images of PPD-5 (left SEM, right TEM).

The SEM of PPD-5 show that spherical nanoassemblies have been formed which are approximately 220 nm in diameter, while TEM (Fig. 4) indicates that small particles of around 20 nm in diameter exist within larger aggregates of around 200 nm. In order to further study the particle morphology, SAXS studies on a 5% w/w dispersion of PPD-5 in methanol were performed (Fig. 5a). In order to simplify the analysis of such complex aggregates, particles were treated as homogeneous solid spheroids. The X-ray intensity of such spheroids, represented by the scattering cross-section per unit sample volume, $\frac{d\Sigma}{d\Omega}(q)$, can be expressed as:

$$\frac{d\Sigma}{d\Omega}(q)_n = N_n S_{PY}(q)_n \int_0^\infty g_{Gauss}(R_n)|F(qR_n)|^2 dR_n \quad \text{(Eq. 1)}$$

where N_n is the number of scatterers, $S_{PY}(q)_n$ is the hard-sphere interaction structure factor based on the Percus-Yevick approximation,[49] $g_{Gauss}(R_n)$ is their Gaussian size distribution function and $F(qR_n)$ is the particle form factor. Specifically, $g_{Gauss}(R_n)$ is expressed as:

$$g_{Gauss}(R_n) = \frac{1}{\sigma_{R_n}\sqrt{2\pi}} e^{-\frac{(R_n - \bar{R}_n)^2}{2\sigma_{R_n}^2}} \quad \text{(Eq. 2)}$$

where $\bar{R}_n$ is the mean radius of the particles and σ_{R_n} is the standard deviation of the size distribution. The particle form factor, $F(qR_n)$, is expressed as:

$$F(qR_n) = \frac{4}{3}\pi {R_n}^3 \Delta\xi \left(3\frac{sin(qR_n) - qR_n cos(qR_n)}{(qR_n)^3}\right) \quad \text{(Eq. 3)}$$

where $\Delta\xi$ is the X-ray scattering contrast.

Initial inspection of the background-subtracted SAXS pattern for a 5% w/w dispersion of PPD-5 in methanol confirmed that a complex morphology was present. Indeed, it

was necessary to account for the presence of two populations of spherical particles: one of small particles (n=1 in Eq. 1-3) and the other of larger particles (n=2 in Eq. 1-3). This approximation provided a satisfactory fit over the majority of the q-range, however an upturn in scattering intensity at low q indicated the presence of larger objects, presumably due to the aggregation of the latter larger aggregates into loose mass fractals as indicated by TEM analysis (Fig. 4). This upturn was modelled using a third population represented by a power law dependence of scattering intensity (Bq^{-p}, where B is a constant and p is an exponent). Thus, the entire scattering pattern is described as:

$$I(q) = \frac{d\Sigma}{d\Omega}(q)_1 + \frac{d\Sigma}{d\Omega}(q)_2 + Bq^{-p} \qquad \text{(Eq. 4)}$$

This three-population approximation provided a satisfactory fit over the entire q-range and indicated that primary nanoparticles of 25.9 ± 19.8 nm in diameter (D_1) existed within larger 194 ± 54.7 nm diameter aggregates (D_2), which themselves exist within loose fractal networks (see Fig. 5b). The Percus-Yevick hard-sphere mean interaction distance between interacting primary particles (D_{PY_1}) is 31.3 nm with a volume fraction of interacting particles of 0.079, and that between larger aggregates (D_{PY_2}) is 270 nm volume fraction of interacting particles of 0.106. Importantly, these dimensions obtained *via* SAXS show good agreement with TEM analysis (Fig. 4).

The porosity of all PPD samples was measured using nitrogen adsorption/desorption at 77 K. The apparent BET surface areas of all PPDs were calculated over the relative pressure range of P/Po = 0.1 – 0.30, which was found to give a positive C value in the BET equation (Table S3, Fig. S9). The apparent BET surface area of the PPD networks range from 11 to 274 m^2/g.

The nitrogen adsorption/desorption isotherm for the solid PPD sample was measured and is presented in figure 6. The isotherm exhibited a steep increase at low relative pressures (P/Po < 0.1), indicative of the presence of micropores within the sample. A very large increase in gas uptake at high pressures (P/Po > 0.9) was also observed. We attribute this to the condensation of nitrogen between particles as might be expected for such aggregated samples. Analysis of the pore size was carried out using the NLDFT method and demonstrated that the sample was indeed microporous with the largest pore size calculated to be centered around 1.8 nm.

The CO_2 uptake was measured at both 298 and 273 K (Fig.6). The PPD was able to uptake *ca*. 1.1 mmol/g of CO_2 at 273 K and 0.7 mmol/g at 298 K. The isosteric heat of adsorption for CO_2 was calculated to be ca. 28 kJ mol^{-1} at low coverage which is comparable to other functionalised microporous polymers.[50,51] Furthermore the selectivity of CO_2/N_2 at 273 K, determined *via* the Henry's Law method, was calculated to be 46.2 (Fig. S10), again comparable to other functionalised microporous polymers.[52]

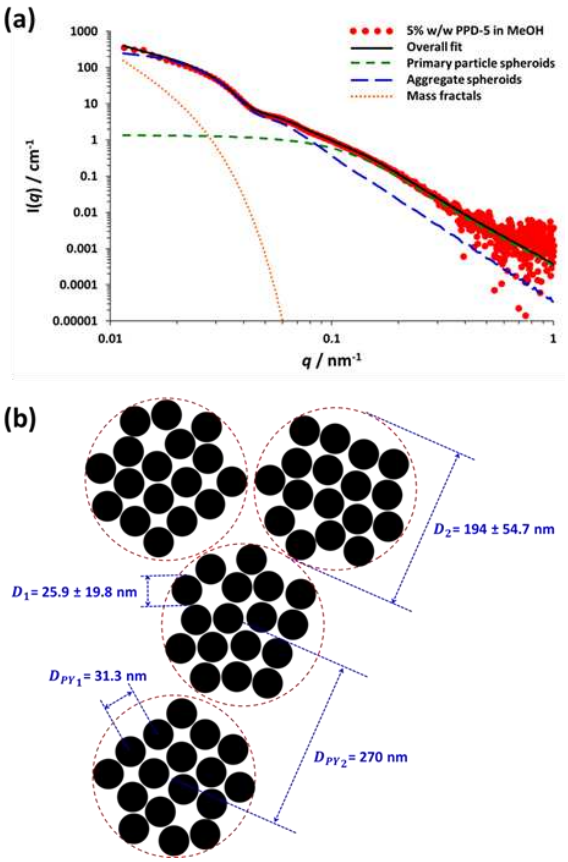

Figure 5. (a) SAXS pattern for a 5% w/w dispersion of the PPD in methanol (red circles) and the overall fit to the data (solid black line), which is the sum three populations: primary particle spheroids (green dashed line), larger aggregate spheroids (blue dashed line) and mass fractals (orange dashed line). (b) Schematic representation of the particle morphology and dimensions of aggregates and their interactions: D_1 is the mean diameter of primary particles, D_2 is the mean diameter of aggregates, D_{PY_1} is the mean interaction distance between primary particles, and D_{PY_2} is the mean interaction distance between larger aggregates.

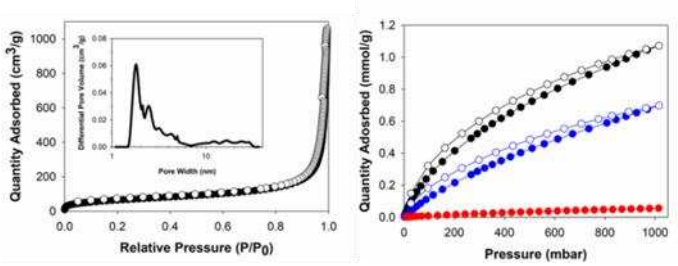

Figure 6. (left) Nitrogen adsorption (filled circles)/desorption (open circles) isotherm for PPD-5 measured at 77 K. Inset: NLDFT pore size distribution (right) CO_2 and N_2 isotherms recorded at 298 K (CO_2 blue), and 273 K CO_2 black and N_2 red)

Figure 7. (Left) Normalized steady state emission spectra of a dispersion of PPD-5 in methanol when exposed to increasing concentrations of picric acid (0-38 ppm). (Middle) An image highlighting the observable fluorescence quenching phenomenon when the PPD is exposed to a nitroaromatic compound. (Right) A histogram highlighting the selectivity of the PPD towards nitroaromatics over other chemically similar compounds (0-200 ppm).

It was found that the PPD samples and the original insoluble FN/DVB analogue fluoresce when exposed to UV light (Fig. 7). Given that the PPD samples are dispersible the fluorescence of the sample was further explored, using PPD-5. Due to the inherent lack of solubility of the FN/DVB analogue exploration of its fluorescence properties were not able to be carried out. Primarily, a UV-vis spectrum of PPD-5, along with that of the monomers, was obtained (Fig. S12). In the case of the PPD, two peaks at 230 and 275 nm are observed. A fluorescence emission spectrum was obtained through excitation at 275 nm wavelength (Fig. S13). This excitation gave rise to emission at *ca*. 325 nm. Upon comparison of the emission spectra of the PPD to the monomers it appears that there is direct overlap between that of DVB and the PPD, with a somewhat broader emission spectrum emanating from the PPD.

Nitroaromatic compounds which are both explosive as well as harmful to the environment, were interestingly found to act as fluorescence quenchers towards the PPDs (Fig. S14). In particular, the need to detect these compounds in waste water streams due to fall-out from chemical industry is vital given their toxicity and danger to both human and aquatic life. Furthermore, these compounds, especially picric acid, pose extreme risk of explosion which is a matter of national security. Hence work was undertaken to evaluate the efficiency and efficacy of the PPD when applied to nitroaromatic detection.

To determine the efficiency of this quenching, fluorescence titration studies were carried out on a range of nitroaromatics (picric acid (PA), nitrobenzene (NB), 2-nitrotoluene (2-NT), 4-nitrotoluene (4-NT), 2,4-dinitrotoluene (2,4-DNT) and 2-nitrophenol (2-NP)). The quenching efficiency (%) was estimated using the formula $(I_o\text{-}I)/I_o \times 100$ where I_o is the maximum fluorescence intensity of the PPD without nitroaromatic compounds. The nitroaromatics studied were all able to quench the fluorescence of the PPDs with efficiencies exceeding 90% when as little as 40 ppm was added to the solution.

To ensure the quenching was selective towards only nitroaromatic compounds, a series of other compounds were investigated implementing the same methodology. The chosen compounds, (chlorobenzene (ClPh), (N,N-dimethylformamide (DMF), toluene (Tol), nitromethane (NM) and benzene (Bz)) all chemically similar to the nitroaromatics studied, were not able to significantly quench the fluorescence of PPD-5 even when added in much larger quantities than the nitroaromatics themselves (Fig S16). This highlights the selective nature of the quenching effect towards the nitroaromatic compounds studied.

Given that the samples synthesised in this work are all porous, the effect porosity plays on the rate of quenching was investigated through studying two PPDs of different surface area (PPD-5 and PPD-2) under identical conditions. It was found that the most porous sample, PPD-5, required much less quencher to achieve the same degree of fluorescence quenching (Fig. S17). This is most likely due to the additional porosity of the PPD allowing faster diffusion of the analyte(s) into the pores.

To probe the quenching mechanism responsible for the chemosensing, Stern-Volmer plots were obtained by plotting Io/I against quencher concentration ([Q]) (Fig. S18). The plots, which deviate from linearity, show that the quenching mechanism is a combination of both static and dynamic effects. Due to both mechanisms being present in the quenching of the system combinational quenching

constants were calculated over a low concentration range (0 – 1 μM) (Fig. S19 and table S4). The trend of quenching constant A for all quenchers followed the order: PA > NB > 2-NT > 4-NT, 2,4-DNT, 2-NP, consistent with the sensitivity of the PPD to the quencher, as shown in figure S15. The limit of detection for PPD-5 (Fig. S19), when exposed to nitroaromatics, was found to be of the order of ppb, with PPD-5/PA having a limit of detection of 169 ppb. This is comparable with other porous polymers possessing fluorescent sensing capabilities.[55,56]

Conclusions

In summary a RAFT-mediated PISA route has been employed in order to develop novel solution processable porous polymeric nanoassemblies. The PPDs synthesised in this work were all shown to be porous and demonstrated long-term stability in a range of organic solvents. The synthesis of the PPDs is one-pot, uses no metal catalysts or environmentally dangerous solvents and is extremely versatile. Furthermore, the PPDs were found to be fluorescent and act as chemosensors towards potentially explosive and toxic nitroaromatic compounds with excellent detection limits. It is our hope that this synthesis will allow for other novel porous and dispersible nanoassemblies to be formed which will pave the way for more interesting and unique porous, solution processable materials.

Acknowledgements

The Leverhulme Trust is thanked for funding of MJD (RPG-2016-330). The authors would like to thank Prof. Julia Weinstein for discussions regarding the luminescence of the particles and Dr. Sandra van Meurs for running solid state NMR experiments. Dr. Oleksandr O. Mykhaylyk is thanked for useful discussions about SAXS analysis. Tom Robshaw is also thanked for attaining SEM images and Dr. Svetomir Tzokov is thanked for TEM assistance.

Notes and references

1 Dawson, R.; Cooper. A. I.; Adams. D. J., Nanoporous Organic Polymer Network, Prog. Polym. Sci., **2012**, 37, 530–563.

2 Boot-Handford, M. E.; Abanades, J.C.; Anthony, E. J.; Blunt, M. J.; Brandani, S.; Mac Dowell, N.; Fernández, J. R.; Ferrari, M. –C.; Gross, R.; Hallett, J. P.; Haszeldine, R. S.; Heptonstall, P.; Lyngfelt, A.; Makuch, Z.; Mangano, E.; Porter, R. T J.; Pourkashanian, M.; Rochelle, G. T.; Shah, N.; Yao J. G.; Fennell, P. S., Carbon Capture and Storgae Update, Energy Environ. Sci., **2014**, 7, 130–189.

3 Wang, W.; Zhou, M.; Yuan, D., Carbon Dioxide Capture in Amorphous Porous Organic Polymers, J. Mater. Chem. A, **2017**, 5, 1334–1347.

4 Yang, X.; Yu, M.; Zhao, Y.; Zhang, C.; Wang, X.; Jiang, J.-X., Hypercrosslinked Microporous Polymers Based on Carbazole for Gas Storage and Separation, RSC Adv., **2014**, 4, 61051–61055.

5 Dawson, R.; Ratvijitvech,; Corker, M.; Laybourn, A.; Khimyak, Y. Z.; Cooper, A. I.; Adams, D. J., Microprous Copolymers for Increased Gas Selectivity, Polym. Chem., **2012**, 3, 2034.

6 Dawson, R.; Stöckel, E.; Holst, J. R.; Adams. D. J.; Cooper, A. I., Microporous Organic Polymers for Carbon Dioxide Capture, Energy Environ. Sci., **2011**, 4, 4239–4245.

7 D'Alessandro, D. M.; Smit, B.; Long, J. R., Carbon Dioxide Capture: Prospects for New Materials, Angew. Chemie Int. Ed., **2010**, 49, 6058–6082.

8 Jiang, K.; Fei, T.; Zhang,T., Humidity Sensing Properties of LiCl-Loaded Porous Polymers With Good Stability and Rapid Response and Recovery, Sensors Actuators, B Chem., **2014**, 199, 1–6.

9 Jiang, K.; Kuang, D.; Fei, T.; Zhang, T., Preparation of Lithium-Modified Porous Polymer for Enhanced Humidity Sensitive Properties, Sensors Actuators, B Chem., **2014**, 203, 752–758.

10 Rakow, N. A.; Wendland, M. S.; Trend, J. E.; Poirier, R, J.; Paoluccia, D. M.; Maki, S. P.; Lyons, C. S.; Swierczek, M. J., Visual Indicator for Trace Organic Volatiles, Langmuir, **2010**, 26, 3767–3770.

11 Dalapati, S.; Jin, S.; Gao, J.; Xu, Y.; Nagai, A.; Jiang, D., An Azine-Linked Covalent Organic Framework, J. Am. Chem. Soc., **2013**, 135, 17310–17313.

12 Tsyurupa, M. P.; Blinnikova, Z. K.; Borisov, Y. A.; Ilyin, M. M.; Klimova, T. P.; Mitsen, K. V.; Davankov, V. A., Physicochemical and Adsorption Properties of Hypercross-linked Polystyrene With Ultimate Cross-linking Density, J. Sep. Sci., **2014**, 37, 803–810.

13 Bratkowska, D.; Davies, A.; Fontanals, N.; Cormack, P. A. G.; Borrull, F.; Sherrington, D. C.; Marcé, R. M., Hypercrosslinked strong Anion-Exchange Resin for Extraction of Acidic Pharmaceuticals From Environmental Water, J. Sep. Sci., **2012**, 35, 2621–2628.

14 Li, R.; Wang, Z. J.; Wang, L.; Ma, B. C.; Ghasimi, S.; Lu, H.; Landfester, K.; Zhang, K. A. I., Photocatalytic Selective Bromination of Electron-Rich Aromatic Compounds Using Microporous Organic Polymers with Visible Light, ACS Catal., **2016**, 6, 1113–1121.

15 Kaur, P.; Hupp, J. T.; Nguyen, S. T., Porous Organic Polymers in Catalysis: Opportunities and Challenges, ACS Catal., **2011**, 1, 819–835.

16 Patel, H. A.; Yavuz, C. T., Noninvasive Functionalization of Polymers of Intrinsic Microporosity for Enhanced CO_2 capture, Chem. Commun., **2012**, 48, 9989.

17 McKeown, N. B.; Budd, P. M.; Msayib, K. J.; Ghanem, B. S.; Kingston, H. J.; Tattershall, C. E.; Makhseed, S.; Reynolds, K. J.; Fritsch, D., Polymers of Intrinsic Microporosity (PIMs): Bridging the Void Between Microporous and Polymeric Materials, Chem. - A Eur. J., **2005**, 11, 2610–2620.

18 Budd, P. M.; Ghanem, B. S.; Makhseed, S.; McKeown, N. B.; Msayib, K. J.; Tattershall, C. E., Polymers of Intrinsic Microporosity (PIMs): Robust, Solution-Processable, Organic Nanoporous Materials, Chem. Commun., **2004**, 230.

19 McKeown, N. B., Polymers of Intrinsic Microporosity, ISRN Mater. Sci., **2012**, 1–16.

20 D. Ramimoghadam, E. M. A. Gray and C. J. Webb, Int. J. Hydrogen Energy, **2016**, 41, 16944–16965.

21 Budd, P. M.; Msayib, K. J.; Tattershall, C. E.; Ghanem, B. S.; Reynolds, K. J.; McKeown, N. B.; Fritsch, D., Gas Separation Membranes From Polymers of Intrinsic Microporosity, J. Memb. Sci., **2005**, 251, 263–269.

22 Xu, Y.; Jin, S.; Xu, H.; Nagai, A.; Jiang, D., Conjugated Microporous Polymers: Design, Synthesis and Application, Chem. Soc. Rev, **2013**, 42, 7965–8178.

23 Sun, C. –J.; Wang, P. –F.; Wang, H.; Han, B. H., All-Thiophene-Based Conjugated Porous Organic Polymers, Polym. Chem., **2016**, 5031–5038.

24 Dawson, R.; Laybourn, A.; Khimyak, Y. Z.; Adams, D. J.; Cooper, A. I., High Surface Area Conjugated Microporous Polymers: The Importance of Reaction Solvent Choice, Macromolecules, **2010**, 43, 8524–8530.

25 Pallavi, P.; Bandyopadhyay, S.; Louis, J.; Deshmukh, A.; Patra, A., A Soluble Conjugated Porous Organic Polymer: Efficient White Light Emission in Solution, Nanoparticles, Gel and Transparent Thin Film, Chem. Commun., **2017**, 53, 1257–1260.

26 Jiang, J. X.; Su, F.; Trewin, A.; Wood, C.D .; Campbell, N. L.; Niu, H.; Dickinson, C.; Ganin, A. Y.; Rosseinsky, M. J.; Khimyak, Y. Z.; Cooper, A. I., Conjugated Microporous Poly(aryleneethynylene) Networks, Angew. Chemie - Int. Ed., **2007**, 46, 8574–8578.

27 Segura, J. L.; Mancheño, M. J.; Zamora, F., Covalent Organic Frameworks Based on Schiff-Base Chemistry: Synthesis, Properties and Potential Applications, Chem. Soc. Rev., **2016**, 45, 5635–5671.

28 A. J. M. and O. M. Y. A. P. Côté, A. I. Benin, N. W. Ockwig, M. O'Keeffe, Science., **2005**, 310, 1166 – 1170.

29 Cote, M. P.; Benin, A. I.; Ockwig, N. W.; O'Keeffe, M.; Matzger, A. J.; Yaghi, O. M., Porous, Crystalline, Covalent Organic Frameworks, Science, **2007**, 316, 268–272.

30 Kuhn, P.; Antonietti, M.; Thomas, A., Porous, Covalent Triazine-Based Frameworks Prepared by Ionotherma; Synthesis, Angew. Chemie - Int. Ed., **2008**, 47, 3450–3453.

31 Puthiaraj, P.; Kim, S. S.; Ahn, W. S., Covalent Triazine Polymers Using A Cyanuric Chloride Precursor via Friedel–Crafts Reaction for CO_2 Adsorption/Separation, Chem. Eng. J., **2016**, 283, 184–192.

32 Reece, C.; Willock, D. J.; Trewin, A., Modelling Analysis of The Structure and Porosity of Covalent Triazine-Based Frameworks, Phys. Chem. Chem. Phys., **2015**, 17, 817–823.

33 Tan, L Tan, B., Hypercrosslinked Porous Polymer Materials: Design, Synthesis, and Applications, Chem. Soc. Rev., **2017**, 46, 3322 – 3356.

34 Tsyurupa, M. P.; Davankov, V. A., H ypercrosslinked Polymers: Basic Principle of Preparing The New Class of Polymeric Materials, React. Funct. Polym., **2002**, 53, 193–203.

35 Dawson, R.; Stevens, L. A.; Drage, T. C.; Snape, C. E.; Smith, M. W.; Adams, D. J.; Cooper, A. I., Impact of Water Coadsorption for Carbon Dioxide Capture in Microporous Polymer Sorbents, J. Am. Chem. Soc., **2012**, 134, 10741–10744.

36 Woodward, R. T.; Stevens, L. A.; Dawson, R.; Vijayaraghavan, M.; Hasell, T.; Silverwood, I. P.; Ewing, A. V.; Ratvijitvech, T.; Exley, J. D.; Chong, S. Y.; Blanc, F.; Adams, D. J. ; Kazarian, S. G.; Snape, C. E.; Drage, T. C.; Cooper, A. I., Swellable, Water- and Acid-Tolerant Polymer Sponges for Chemoselective Carbon Dioxide Capture, J. Am. Chem. Soc., **2014**, 136, 9028–9035.

37 Martin, C. F.; Stockel, E.; Clowes, R.; Adams, D. J. ; Cooper, A. I.; Pis, J. J.; Rubiera, F.; Pevida, C., Hypercrosslinked Organic Polymer Networks as Potential Adsorbents for Pre-Combustion CO_2 Capture, J. Mater. Chem., **2011**, 21, 5474–5483

38 Li, B.; Gong, R.; Wang, W.; Huang, X.; Zhang, W.; Li, H.; Hu, C.; Tan, B., A New Strategy to Microporous Polymers: Knitting Rigid Aromatic Building Blocks by External Cross-Linker, Macromolecules, **2011**, 44, 2410–2414.

39 Deshmukh, A.; Bandyopadhyay, S.; James, A.; Patra, A., Trace Level Detection of Nitroanilines Using A Solution Processable Fluorescent Porous Organic Polymer, J. Mater. Chem. C, **2016**, 4, 4427–4433.

40 Cheng, G.; Hasell, T.; Trewin, A.; Adams, D. J.; Cooper, A. I., Soluble Conjugated Microporous Polymers, Angew. Chemie - Int. Ed., **2012**, 51, 12727–12731.

41 Yang, Y.; Tan, B.; Wood, C. D., Solution-Processable Hypercrosslinked Polymers by Low Cost Strategies: A Promising Platform for Gas Storage and Separation, J. Mater. Chem. A, **2016**, 4, 15072–15080.

42 Mai, W.; Sun, B.; Chen, L.; Xu, F.; Liu, H.; Liang, Y.; Fu, R.; Wu, D.; Matyjaszewski, K., Water-Dispersible, Responsive, and Carbonizable Hairy Microporous Polymeric Nanospheres, J. Am. Chem. Soc., **2015**, 137, 13256–13259.

43 Xie, F.; Hu, W.; Ding, L.; Tian, K.; Wu, Z.; Li, L.; Polym. Chem., Synthesis of Microporous Organic Polymers via Radical Polymerization of Fumaronitrile with Divinylbenzene, **2017**, 8, 6106–6111.

44 Pangborn, A. B.; Giardello, M. A.; Grubbs, R. H.; Rosen, R. K.; Timmers, F. J., Safe and Convenient Procedure for Solvent Purification, Organometallics, **1996**, 15, 1518–1520.

45 Chen, J.; Liu, M.; Gong, H.; Huang, Y.; Chen, C., Synthesis and Self-Assembly of Thermoresponsive PEG-b-PNIPAM-b- PCL ABC Triblock Copolymer through the Combination of Atom Transfer Radical Polymerization, Ring-Opening Polymerization, and Click Chemistry, J. Phys. Chem. B, **2011**, 115, 14947–55.

46 Skey, J.; O'Reilly, R. K., Facile One Pot Synthesis of A Range of Reversible Addition Fragmentation Chain Transfer (RAFT) Agents, Chem. Commun., **2008**, 4183.

47 Trent, J. S., Ruthenium Tetraoxide Staining of Polymers: New Preparative Methods for Electron Microscopy, Macromolecules, **1984**, 17, 2930–2931.

48 Ilavsky, J.; Jemian, P. R., Irena: Tool Suite for Modeling and Analysis of Small-Angle Scattering, J. Appl. Crystallogr., **2009**, 42, 347–353.

49 Kinning, D. J.; Thomas, E. L., Hard-Sphere

Interactions between Spherical Domains in Diblock Copolymers, Macromolecules, **1984**, 17, 1712–1718.

50 Chen, D.; Gu, S.; Fu, Y.; Zhu, Y.; Liu, C.; Li, G.; Yu, G.; Pan, C., Tunable Porosity of Nanoporous Organic Polymers With Hierarchical Pores for Enhanced CO_2 Capture, Polym. Chem., **2016**, 7, 3416–3422.

51 Choma, J;. Stachurska, K.; Marszewski, M.; Jaroniec, M., Equilibrium Isotherms and Isosteric Heat for CO_2 Adsorption on Nanoporous Carbons from Polymers, Adsorption, **2016**, 22, 581–588.

52 Dawson, R.; Cooper, A. I.; Adams, D. J., Chemical Functionalization Strategies for Carbon Dioxide Capture in Microporous Organic Polymers, Polym. Int., **2013**, 62, 345–352.

53 Pramanik, S.; Zheng, C.; Zhang, X.; Emge, T. J.; Li, J., New Microporous Metal-Organic Framework Demonstrating Unique Selectivity for Detection of High Explosives and Aromatic Compounds, J. Am. Chem. Soc., **2011**, 133, 4153–4155.

54 Sun, X.; Wang. Y.; Lei, Y., Fluorescence Based Explosive Detection: From Mechanisms to Sensory Materials, Chem. Soc. Rev., **2015**, 44, 8019–8061.

55 Ma, H.; Li, B.; Zhang, L.; Han, D.; Zhu, G., Targeted Synthesis of Core–Shell Porous Aromatic Frameworks for Selective Detection of Nitro Aromatic Explosives via Fluorescence Two- Dimensional Response, J. Mater. Chem. A, **2015**, 3, 19346–19352.

56 Sun, R.; Huo, X.; Lu, H.; Feng, S.; Wang, D.; Liu, H., Recyclable Fluorescent Paper Sensor for Visual Detection of Nitroaromatic Explosives, Sens. Actuators B Chem., **2018**, 265, 476–487.

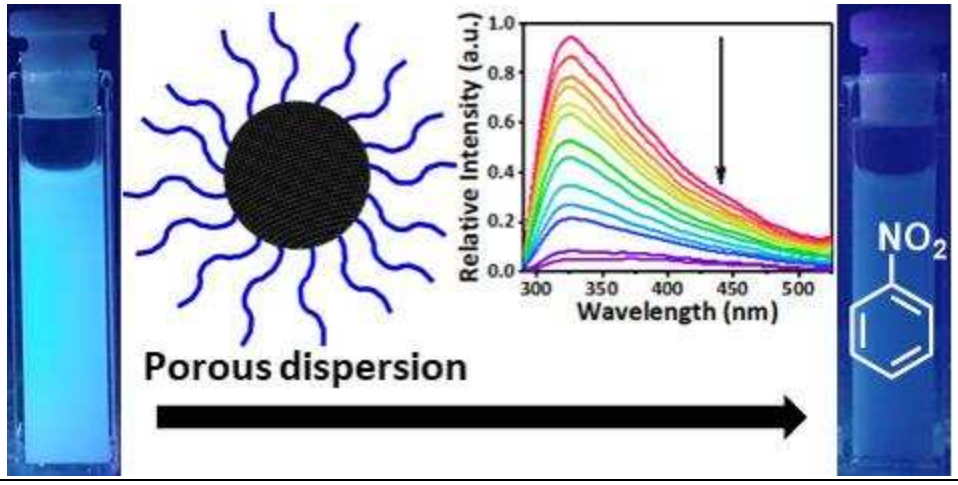
Relative Intensity (a.u.)
1.0
0.8
0.6
0.4
0.2
0.0
300
350
400
450
500
Wavelength (nm)
Porous dispersion
NO2